PAPER

N,N-Dimethylaminoethyl methacrylate-based core/shell microgels loaded with silver nanoparticles for catalysis†

Muhammad Khizar Hyat, [a] Prashun Ghosh Roy, [b] Muhammad Azam, [a] Shuiqin Zhou, [b] Ahmad Irfan, [c] Nayab Batool Rizvi, [a] Robina Begum [*a] and Zahoor H. Farooqi [*a]

In this work, poly(styrene)@poly(*N*-isopropylmethacrylamide-*co*-2-(*N,N*-dimethyl)aminoethyl methacrylate [p(sty)@p(NIPMAM-DMAEMA)] core/shell microgel particles were produced by a two-step free-radical precipitation polymerization process. Ag nanoparticles were successfully embedded inside the sieves of a crosslinked network by using silver nitrate as the precursor salt and NaBH$_4$ as the reductant. The synthesized pure and hybrid microgels were analyzed by various characterization tools, including Fourier transform infrared (FTIR) and UV-visible (UV-vis) spectroscopies, transmission electron microscopy (TEM) and dynamic light scattering (DLS). Results indicate the successful fabrication of spherical silver nanoparticles with diameters ranging from 10 to 15 nm within the sieves of the poly(styrene)@poly(*N*-isopropylmethacrylamide-*co*-2-(*N,N*-dimethyl)aminoethyl methacrylate) core/shell microgels, which have a hydrodynamic diameter of 155 ± 25 nm. The Ag nanomaterial exhibited long-term stability in the p(sty)@p(NIPMAM-DMAEMA) system due to the strong donor–acceptor relationship between the lone pair of the amide moiety in the polymer microgels and the Ag nanomaterial. The catalytic activity of the Ag-p(sty)@p(NIPMAM-DMAEMA) material was determined by performing the catalytic reduction of *p*-nitrophenol (4-NPh) as a model reaction under diverse concentrations of the catalyst. UV-vis spectrophotometry was used to check the progress of the reaction. The apparent rate constant (k_{app}) was measured by applying the pseudo-first-order kinetics model. It was observed that k_{app} increased with increasing catalyst dose, demonstrating occurrence of the reaction on the surface of the catalyst.

1. Introduction

Silver nanomaterials have gained significant attention worldwide owing to their distinct physical and chemical properties and their potential uses in various fields.[1] Their extraordinary features comprise optical[2] and electronic[3] properties, excellent thermal conductivities[4] and biological features.[5] As a result of these unique features, silver nanomaterials find applications in catalysis,[6,7] medicine,[8] cosmetics,[9] human healthcare,[10] sensing,[11] bio-sensing,[12] drug carriers,[13] water treatment,[14] textile industries,[15] and antibacterial,[16] antifungal,[17] anticancer[18] and antiviral systems.[19]

Silver nanoparticles (AgNPs) are well known for their catalytic activity. Their small size and huge surface-to-volume ratio provide abundant active sites and unique electronic properties, which make them highly valuable and efficient catalysts.[20,21] This has fueled extensive research on utilizing AgNPs as catalysts in diverse chemical processes, such as organic transformations and degradations of toxic chemicals. However, achieving stable silver nanoparticles is a highly challenging task as they are not very stable in their naked state because of their high surface energy and undergo agglomeration over time, which reduces their catalytic efficiency and impedes their practical applications.[22] To overcome this problem, many stabilizing systems, such as polymer brushes,[23] dendrimers,[24,25] micelles,[26] surfactants,[27] polyelectrolytes[28] and microgels[29,30] have been used. Among them, smart microgels are the best for nanoparticle stabilization due to their protective matrices and highly cross-linked networks. They keep the metal nanoparticles apart and prevent the aggregation of nanoparticles. Moreover, microgels are preferred due to their facile synthesis,

aSchool of Chemistry, University of the Punjab, New Campus, Lahore 54590, Pakistan. E-mail: robina.hons@pu.edu.pk; robina.chem@pu.edu.pk; zahoor.chem@pu.edu.pk; zhfarooqi@gmail.com

bDepartment of Chemistry of The College of Staten Island and PhD Program in Chemistry of The Graduate Centre, The City University of New York, 2800 Victory Boulevard, Staten Island, NY 10314, USA

cDepartment of Chemistry, College of Science, King Khalid University, P.O. Box 9004, Abha 61413, Saudi Arabia

multiple sensitivity or selectivity, low cost, high stability, non-toxicity, excellent re-usability, easy functionalization, unique morphologies and uniform size distribution. The dimension of the AgNPs can be controlled and attuned as required by altering the size of the sieves in the microgel particles. Copolymer microgels obtained by the polymerization of NIPMAM and DMAEMA in the presence of a crosslinker, and their application as micro-reactors for the synthesis of metal nanomaterials for catalysis have not been reported in literature previously. While p(NIPMAM-DMAEMA) microgels and their hybrids are difficult to recover at low centrifugation speeds, core/shell microgels with a solid poly(styrene) core and p(NIPMAM-DMAEMA) shell and their hybrids can be easily recovered by ordinary centrifugation. Due to the aforementioned characteristics, the synthesis and stabilization of various metal nanoparticles in smart polymer microgels fabricated with various combinations of monomers and co-monomers have been extensively described in the literature.[31,32]

Rehman et al.[33] prepared poly(NIPAM-co-DMAEMA) cross-linked microparticles by free-radical precipitation polymerization and used the synthesized microgels as micro-reactors for the fabrication of Au nanoparticles within the network. They used the prepared hybrid microgels for the catalytic reduction of p-nitrophenol at various temperatures. The values of the apparent rate constant (k_{app}) were thermally tunable based on the volume phase transition temperature (VPTT) of the microgels. Huang et al.[34] reported a reductant-free method for the fabrication of Ag nanoparticles within a micellar system obtained from amphiphilic star-shaped copolymers composed of p(ε-caprolactone), 2-(dimethylamino)ethyl methacrylate and oligo(ethylene glycol)monomethyl ether methacrylate units. The 2-(dimethylamino)ethyl methacrylate units were used as the reductant for the production of Ag nanoparticles when the nitrogen atom was deprotonated (pH > 7), allowing the nitrogen atom to donate the lone pairs of electrons to Ag^+ ions and reduce them to zero valent silver [Ag(0)]. These Ag nanoparticles were spherical with diameters in the range of 10–20 nm and were stabilized by star-shaped copolymers. Reddy et al.[35] prepared a chitosan@poly(DMAEMA-HEMA) hydrogel by simple precipitation polymerization and fabricated a hydrogel system with Ag nanoparticles using $NaBH_4$ as the reductant. Both pure and hybrid hydrogels were loaded with the drug amoxicillin. The results showed that the amoxicillin-loaded hybrid hydrogels have an improved ability to cleave DNA and good anti-microbial activity.

Therefore, special interest is given to DMAEMA-based microgels as these contain tertiary amine groups, which are basic in nature and make the polymeric system pH sensitive. Temperature sensitivity can be incorporated by using suitable thermosensitive units along with DMAEMA. Zha et al.[36] published the production of p(NIPAM-DMAEMA) homogeneous microgels with both temperature sensitivity and pH sensitivity. NIPMAM is also thermosensitive just like NIPAM, but the VPTT (44–46 °C) of p(NIPMAM) microgels are higher than the VPTT (32 °C) of p(NIPAM) microgels in water. To the best of our knowledge, the preparation, characterization, and catalytic

action of Ag-p(sty)@p(NIPMAM-DMAEMA) core/shell hybrid microgels have not been reported previously.

In this study, p(sty)@p(NIPMAM-DMAEMA) microparticles with a p(sty) core and a p(NIPMAM-DMAEMA) shell were obtained by a seed-mediated free-radical precipitation polymerization, and Ag nanoparticles were loaded in the meshes of the shell region of the microgels by a chemical reduction method. The catalytic ability of the resultant hybrid microgel system was checked by reducing the p-nitrophenol into 4-aminophenol at different catalyst doses.

2. Experimental

2.1 Material

N-Isopropylmethacrylamide (NIPMAM, 98%), 2-(N,N-dimethyl-amino)ethyl methacrylate (DMAEMA, 98%), styrene (sty), N,N-methylenebis(acrylamide) (bis, 99%), sodium dodecyl sulfate (SDS, 98%), ammonium persulfate (APs, 99%), and sodium borohydride ($NaBH_4$, 98%) were received from Sigma-Aldrich, Germany. The purchase of silver nitrate ($AgNO_3$, 97%) was made from Gemistone Chemicals. All obtained chemicals, except for styrene, were used as received without any additional purification. To remove the inhibitor, styrene was subjected to vacuum filtration by passing through alumina (Al_2O_3). The synthesis of p(sty)@p(NIPMAM-DMAEMA) and Ag-p(sty)@p(NIPMAM-DMAEMA), as well as the catalytic process, were done using de-ionized water. For the purification of the microgels and hybrid microgels, a dialysis membrane with a cut-off range between 12 000 and 14 000 dalton, received from Fischer Scientific UK, was utilized.

2.2 Synthesis

2.2.1. Synthesis of the poly(styrene) core particles. The poly(styrene) core latex particles were produced by free-radical precipitation polymerization using styrene (monomer), NIPMAM (co-monomer), SDS (emulsifier), and APs (initiator), as described in our previous works.[37,38] 0.108 g NIPMAM (0.85 mmol, 5 mol%), 1.85 mL styrene (16.15 mmol, 95 mol%; density = 0.909 g mL^{-1}), 0.05 g SDS, and 90 mL water were placed in a round-bottom flask. The mixture was agitated for 15 minutes under an N_2 environment. The temperature was raised to 80 °C, and then the mixture was heated at this temperature for 35 minutes. Then, 9.0 mL of APs solution (0.064 M) was injected into the reaction vessel, and the process was continued further for six hours under stirring, heating, and N_2 flow until the polymerization process was completeted. The prepared p(styrene) core microparticle dispersion was purified by dialysis to eliminate unreacted moieties via dialysis of the surfactant (SDS), initiator (APs) and monomers.

2.2.2. Preparation of p(sty)@p(NIPMAM-DMAEMA). The p(sty) core latex particles were employed as seeds for the construction of a p(NIPMAM-DMAEMA) network around them to obtain p(sty)@p(NIPMAM-DMAEMA) microparticles. The purpose of the crosslinked thin layer formation around the p(sty) particles was to bind the AgNPs in the formed outer layer for minimizing the mass transport obstacle encountered by the

reactant molecules during catalysis. For the fabrication of a thin shell layer, 33 mL deionized water, 0.598 g NIPMAM (94 mol%), 0.015 g bis (2 mol%), 0.031 g (833 μL) DMAEMA (4 mol%), 0.04 g SDS and 17 mL p(sty) dispersion were mixed in a round-bottom flask and agitated for 5 min under N_2 purging. The temperature of the reaction mixture was maintained at 71 °C while nitrogen was supplied continuously. After 30 min at this temperature and constant stirring, 2.5 mL of an APs solution (0.080 M) was injected into the mixture, and the reaction was continued further for 4.5 h. The synthesized p(sty)@p(NIPMAM-DMAEMA) dispersion was purified *via* dialysis to remove unreacted species, such as the crosslinker, monomers, emulsifier and initiator.

2.2.3. Fabrication of p(sty)@p(NIPMAM-DMAEMA) hybrids. A mixture of 8 mL of the as-fabricated p(sty) @(NIPMAM-DMAEMA) microgel dispersion and 35 mL of pure water was agitated under N_2 environment in a round-bottom flask placed in ice-cold water to maintain a temperature of 0 °C. To this, 0.30 mL of an aqueous silver nitrate solution (0.1 M) was introduced, and stirring was continued for 10 minutes under nitrogen purge. Then, freshly prepared 6.7 mL $NaBH_4$ solution (0.04 M) was transferred dropwise into the microgel dispersion loaded with silver ions, and the process was continued for 30 minutes under continuous N_2 purging. A brownish dispersion of microgels loaded with silver nanoparticles was formed, and it was purified by dialysis for 20 minutes against distilled water.

2.3 Characterization

Individual dispersions of p(sty), p(sty)@p(NIPMAM-DMAEMA), and Ag-p(sty)@p(NIPMAM-DMAEMA) particles were dried for 12 hours in an oven at 70 °C. Then, the samples were collected in the form of powder and subjected to FTIR analysis using an RXI FTIR spectrometer (PerkinElmer, USA) to determine the functionalities present in the samples. The UV-vis spectra of the core, core/shell, and hybrid systems were recorded in the wavelength region of 200–800 nm at 20 °C using an SP-UV 500 DB/VDB spectrophotometer. Stability of the hybrid microgel and catalysis progression were also monitored by UV-vis spectrophotometry. TEM micrographs were captured by using a Fei Tecnai transmission electron microscope operated at 120 kV. The diluted suspension of each sample was air-dried on a carbon-coated copper grid to produce TEM images. The

hydrodynamic radii of the p(sty) and p(sty)@p(NIPMAM-DMAEMA) particles were determined as a function of temperature (20–45 °C) using a DLS spectrometer (BI-200SM equipped with BI-9000 AT, Brookhaven Instruments, Inc.). A helium-neon laser (35.0 mW, 633 nm) was employed as the source of light. Dust particles were removed by passing each dispersion through a Millex-HV Millipore filter with a pore diameter of 0.45 μm before DLS measurements.

2.4 Catalytic studies

The catalytic potential of the Ag-p(sty)@p(NIPMAM-DMAEMA) system (0.2020 mg mL^{-1}) was tested in the reduction of 0.06 mM 4-NPh by 15 mM $NaBH_4$ in a water medium. This reaction was also carried out using different concentrations of the catalyst. Similarly, 2.5 mL reaction solutions containing other nitroarenes (0.06 mM), 15 mM $NaBH_4$, and 0.1616 mg mL^{-1} of the Ag-p(sty)@p(NIPMAM-DMAEMA) catalyst were taken in a quartz cuvette for UV-visible spectrophotometric monitoring of the reaction in the wavelength range of 200–600 nm at 30 °C.

3. Results and discussion

3.1 Engineering of the p(sty) core latex particles and p(sty) @p(NIPMAM-DMAEMA) particles

The poly(styrene) core latex particles and p(sty)@p(NIPMAM-DMAEMA) core/shell microgel particles were obtained by the precipitation polymerization method. The schematic of the preparation process is given in Fig. 1. In the initial step, the poly(styrene) core was prepared using styrene (monomer), NIPMAM (*co*-monomer), water (reaction medium), SDS (emulsifier), and APs (initiator) by free-radical emulsion polymerization method. In the second step, the seed-mediated emulsion polymerization method was employed for building a thin layered shell around the p(styrene) core latex particles. A small quantity of NIPMAM was used during the initial step to promote the stability of the poly(styrene) core and induce charge, creating a strong interaction between the core latex and the outer shell region. As the poly(styrene) core is hydrophobic in nature, so the shell was synthesized at a high temperature of around 80 °C. The high temperature increased the hydrophobicity of p(NIPMAM-DMAEMA) during the polymerization of NIPMAM and DMAEMA in the presence of the p(sty) seeds.
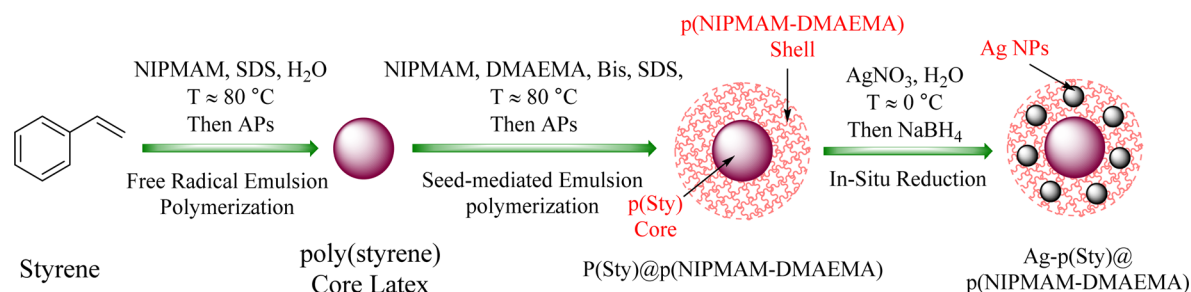

Fig. 1 Graphical representation of the synthesis of p(sty) core, p(sty)@p(NIPMAM-DMAEMA) core/shell microgels and Ag-nanoparticle-loaded p(sty)@p(NIPMAM-DMAEMA) core/shell hybrid microgels.

Therefore, a strong affinity between the p(sty) core and the p(NIPMAM-DMAEMA) shell was established due to the improved hydrophobicity of the shell at high temperatures.

3.2 Preparation of the Ag-p(sty)@p(NIPMAM-DMAEMA) hybrids

For the fabrication of the Ag nanomaterial in the shell region of the prepared p(sty)@p(NIPMAM-DMAEMA), a chemical reduction route was employed. In this process, $AgNO_3$ salt was used as the Ag^+ ion source, while $NaBH_4$ was used as the reducing agent. Ag^+ ions were loaded into the thin layered shell of the pure microgels at a very low temperature (around 0 °C, which is much lower than the VPTT of the microgel). The low temperature kept the microgel particles in a swollen state and made the migration of Ag^+ ions from the bulk solution to the polymeric network easier. The silver ions were attracted to the polymeric system because of the donor–acceptor interaction between the Ag^+ ions and the amide and tertiary amine groups of the p(NIPMAM-DMAEMA) shell network. Such donor–acceptor interaction has also been reported previously between the carbonyl groups (C=O) of the acrylate moiety of DMAEMA and Ag^+ ions.[39,40] In the sieves of the shell region, monovalent Ag^+ ions were reduced by sodium borohydride to zerovalent silver atoms. The reduced Ag atoms aggregated in the cavities of the polymer network to form clusters. These clusters immediately combined with one another to form Ag nanoparticles. The change in color of the turbid microgel dispersion from milky white to brownish green in the reaction mixture confirmed the formation of AgNPs.

3.3 Characterization

The FTIR spectra of the p(sty), p(sty)@p(NIPMAM-DMAEMA), and Ag-p(sty)@p(NIPMAM-DMAEMA) samples are given in Fig. 2. An absorption peak appeared at 3250 cm^{-1} in the IR spectrum of the core/shell microgel system due to amide N–H stretching in the NIPMAM units, and this absorption became stronger, broader, and shifted to a slightly higher wavenumber in the hybrid microgel spectrum due to the physical interaction of the silver metal nanoparticles with the N–H group. Another prominent absorption peak was detected at 1626 cm^{-1} due to

C=O (carbonyl group) stretching in both core/shell microgels as well as hybrid microgels. No absorption peak at 1550–1600 cm^{-1} was observed which is a proof that C=C had transformed into a C–C bond and the polymerization process was successfully completed. In the FTIR spectra, the two absorption peaks at 1523 cm^{-1} and 1459 cm^{-1} are due to C=C stretching in the aromatic ring of the p(styrene) core.

The UV-vis spectra of the dispersions of p(sty), p(sty)@p(NIPMAM-DMAEMA) and Ag-p(sty)@p(NIPMAM-DMAEMA) are displayed in Fig. 3. The dilute dispersions of the pure core, pure microgels and pure hybrids were measured in the wavelength range of 230–800 nm. There was no band in the visible-light region of the UV-vis spectra of the pure core and the pure microgel system, but the dispersion of hybrid microgels had a single band at 404 nm due to the characteristic collective oscillation of the surface electrons of the silver nanoparticles, which is also known as SPR (Surface Plasmon Resonance) and indicates that spherical Ag nanoparticles were successfully fabricated in the sieves of the outer region of p(sty)@p(NIPMAM-DMAEMA). During the fabrication process, a color change from milky white to light brown was observed, indicating that Ag nanoparticles were successfully fabricated within the dispersion of microgels.

TEM examination of the samples was carried out to determine the morphology, size, and core size distribution in the core/shell microgels, and Ag nanoparticle loading inside the sieves of core/shell microgels. The TEM images of p(sty), p(sty)@p(NIPMAM-DMAEMA) and Ag-p(sty)@p(NIPMAM-DMAEMA) particles are presented in Fig. 4(A–D). Fig. 4(A) shows spherical core particles with a diameter of 143 nm; Fig. 4(B) and (C) show p(sty)@p(NIPMAM-DMAEMA) particles with a diameter of 155 nm at different resolutions, and Fig. 4(D) depicts the hybrid microgel particles. The small spherical black dots in Fig. 4(D) are Ag nanoparticles with a diameter range of 10–15 nm fabricated both inside and on the shell surface of the polymer particles. The value of thickness of shell of p(sty)@p(NIPMAM-DMAEMA) particles was evaluated from the difference in diameters between the core/shell and core particles, and it was found to be 12 nm. The TEM micrograph of the Ag-p(sty)
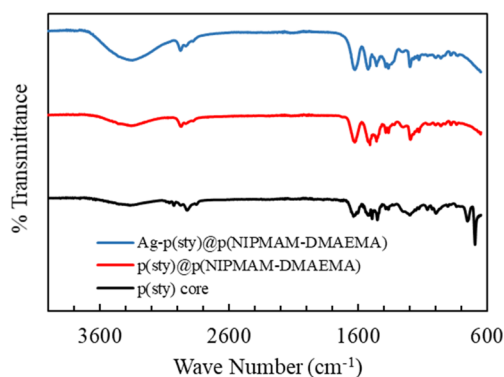

Fig. 2 FT-IR spectra of p(sty) core, pure p(sty)@p(NIPMAM-DMAEMA) microgel and Ag-p(sty)@p(NIPMAM-DMAEMA) hybrid microgels.
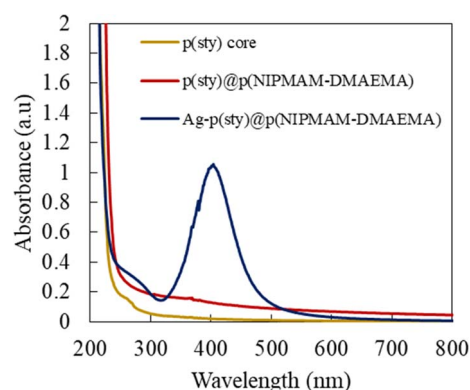

Fig. 3 UV-vis spectra of dilute dispersions of p(sty), p(sty)@p(NIPMAM-DMAEMA) and Ag-p(sty)@p(NIPMAM-DMAEMA) at room temperature in an aqueous medium.
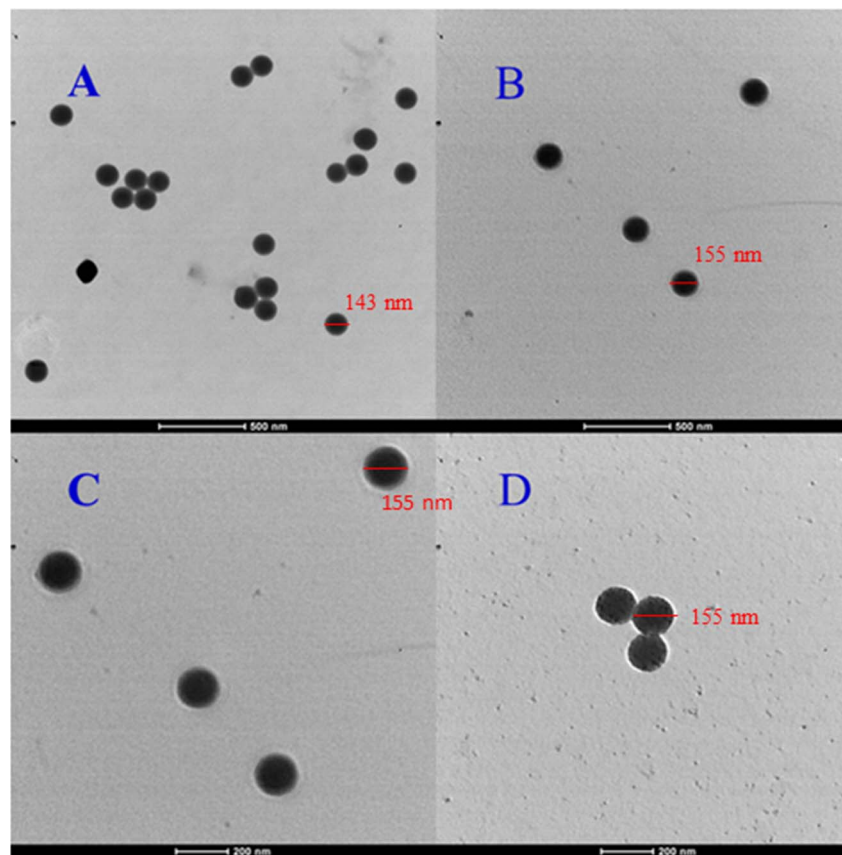
Fig. 4 TEM images of p(sty) (A), p(sty)@p(NIPMAM–DMAEMA) (B and C) and Ag-p(sty)@p(NIPMAM–DMAEMA) (D).

@p(NIPMAM-DMAEMA) system, as shown in the inset of Fig. S1 (ESI),† was used for the size estimation of the silver nanoparticles present in p(sty)@p(NIPMAM-DMAEMA).

It is worth mentioning that no change in the radius of p(sty) @p(NIPMAM-DMAEMA) particles was observed after the fabrication of Ag nanoparticles in the shell region (Fig. 4C and D). The hydrodynamic diameters (D_h) of p(sty) and p(sty)

@p(NIPMAM-DMAEMA) particles were determined using DLS measurements of the respective dilute dispersions. Fig. 5(A) gives the plot of D_h as a function of temperature in aqueous p(sty) and p(sty)@p(NIPMAM-DMAEMA) systems. It is evident from Fig. 5(A) that the D_h value of the p(sty) particles remained constant in the investigated temperature range due to the temperature insensitivity of the p(sty) core particles. However,
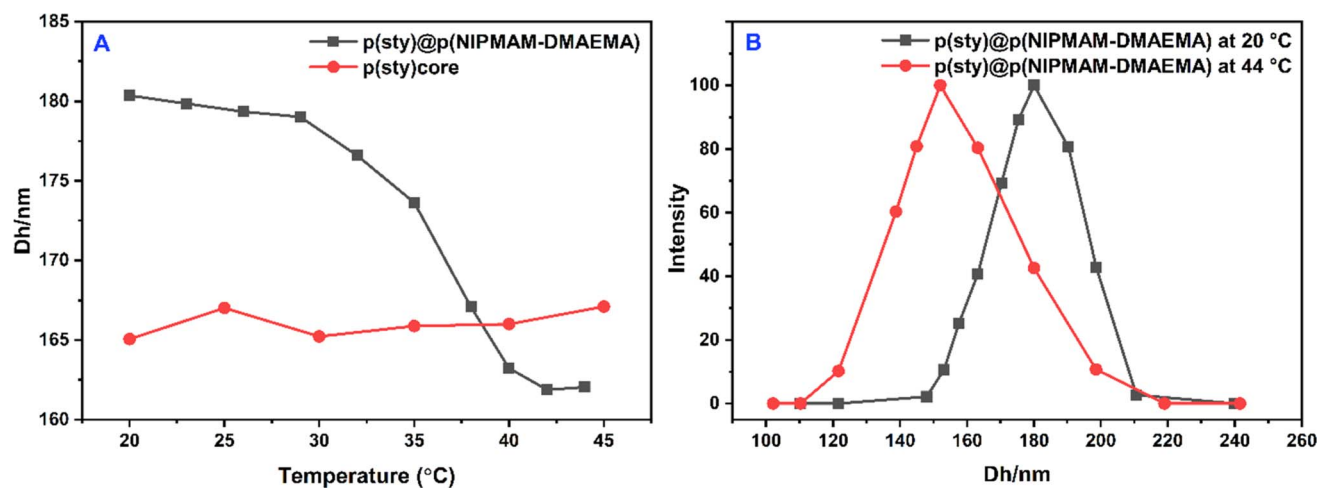

Fig. 5 Hydrodynamic radius of p(sty) core particles and p(sty)@p(NIPMAM–DMAEMA) core/shell particles as a function of temperature (A) and particle size distribution of the p(sty)@p(NIPMAM–DMAEMA) core/shell particles at two different temperatures (B).

the D_h value of the p(sty)@p(NIPMAM-DMAEMA) particles decreased with a rise in temperature from 20 °C to 42 °C in water, which may be attributed to the thermosensitive behavior of the NIPMAM units of the core/shell microgels. Interestingly, the variation in D_h value with temperature was significant in the temperature range of 30–42 °C. This drastic decrease in D_h value may be attributed to the breakage of hydrogen bonding between the functionalities of NIPMAM units and the water molecules. The value of VPTT of the p(sty)@p(NIPMAM-DMAEMA) system was found to be around 36–38 °C, which is very close to the physiological temperature (37 °C), making the system suitable for future biomedical applications. The VPTT of the present system is lower than the VPTT of P(NIPMAM)-based microgels reported in the literature.[41] The presence of the hydrophobic p(sty) core in the central region and DMAEMA units in the shell region may have caused this shift in the VPTT of the microgel system. The D_h values of the p(sty), p(sty)@p(NIPMAM-DMAEMA), and Ag-p(sty)@p(NIPMAM-DMAEMA) systems were slightly higher than those measured by TEM at room temperature, which may be due to swelling of particles in the aqueous medium. Fig. 5(B) gives the size distribution curves of the p(sty)@p(NIPMAM-DMAEMA) core/shell system at two different temperatures in water. The size distribution of the p(sty)@p(NIPMAM-DMAEMA) system broadens at $T \geq$ VPTT due to non-homogeneous heating, but the most probable value of D_h at 44 °C (162.03 nm) is lower than the value of D_h at 20 °C (180.37 nm). It has previously been reported by us and others that loading metal nanoparticles do not affect the thermoresponsive behavior of a pure microgel system. It is important to mention the microgel system almost remained in a swollen state (with an open network) from 20 °C to 30 °C. Therefore, p(sty)@p(NIPMAM-DMAEMA) may be considered as a catalyst without the diffusional barrier faced by reactant molecules at $T \leq$ VPTT. Therefore, catalytic experiments were performed in this temperature range.

To check the stability of the Ag nanoparticles over time, the UV-vis spectra of freshly prepared and 120 days-old Ag-p(sty)@p(NIPMAM-DMAEMA) hybrid microgels were scanned and are displayed in Fig. 6. The graphs show that the position of the

Fig. 6 UV-vis spectra of the freshly prepared dilute dispersion of Ag-p(sty)@p(NIPMAM-DMAEMA) hybrid microgels and hybrid microgels stored for four months.

surface plasmon resonance wavelengths (λ_{SPR}) of both freshly synthesized and 120 days-old hybrid microgels remained the same, but the absorption intensity of the 120 days-old hybrid microgels was slightly decreased, which may be attributed to the adsorption of hybrid particles to the wall of the vial over time. This indicates that the Ag nanoparticles are highly stable in the external region of the p(sty)@p(NIPMAM-DMAEMA) microgels.

Furthermore, there was no variation in the color of the hybrid microgel dispersion with time, which is also an indication that the fabricated silver nanoparticles have good stability in the network.

3.4 Catalytic potential of Ag-p(sty)@p(NIPMAM-DMAEMA)

The catalytic potential of Ag-p(sty)@p(NIPMAM-DMAEMA) was studied through its application as a catalyst in the conversion of *p*-nitrophenol (4-NPh) into *p*-aminophenol (4-APh) by utilizing NaBH$_4$ as the reducing agent in water medium. This reduction reaction has great significance and is extensively used as an exemplary reaction for assessing the catalytic efficiency of many nanocatalytic systems. From the environmental perspective, it is vital to convert 4-NPh to 4-APh. 4-NPh is an extremely hazardous material and is a by-product of numerous industrial processes. On the other hand, 4-APh is less hazardous than 4-NPh and is frequently used as a reactant in the synthesis of various organic dyes. Furthermore, UV-vis spectrophotometry was used to monitor the transformation of 4-NPh to 4-APh. This method is effective because both the starting material and the final product absorb light in the UV-visible range with a sufficient gap between their wavelengths of maximum absorption (λ_{max}) at basic pH. In the presence of a reductant (NaBH$_4$), the acidic proton of *p*-nitrophenol is removed, and a *p*-nitrophenolate ion is formed (λ_{max} = 398 nm). Additionally, the reaction of 4-NPh and NaBH$_4$ without a catalyst is thermodynamically spontaneous in the water medium, but it is not kinetically very favorable. It becomes kinetically favorable only in the presence of a catalyst. Therefore, it was used to test the catalytic activity of the nanoparticle-based catalytic system. The catalyst used in this reaction can be recycled easily by centrifugation with only a minute decline in the catalytic activity because all reactants and products were water soluble. Our group has already reported the catalytic activity of microgels containing metal nanoparticles using the reduction of 4-NPh by NaBH$_4$ as the model reaction.[42–44]

Before investigating the detailed catalytic activity of the Ag-p(sty)@p(NIPMAM-DMAEMA) hybrid system, various control experiments were carried out. As a control experiment, the reduction of 4-NPh by sodium borohydride in water was tested without the Ag-p(sty)@p(NIPMAM-DMAEMA) hybrid microgels, as shown in Fig. 7. The value of absorbance at λ_{max} did not decrease significantly, and the yellow color of *p*-nitrophenolate persisted, which is a clear indication that reduction did not take place without Ag-p(sty)@p(NIPMAM-DMAEMA). However, in the presence of the Ag-p(sty)@p(NIPMAM-DMAEMA) hybrid microgels, an observable change occurred in the reaction mixture. Specifically, the color of the reaction mixture changed from yellow to colorless within 30 minutes. This change in color
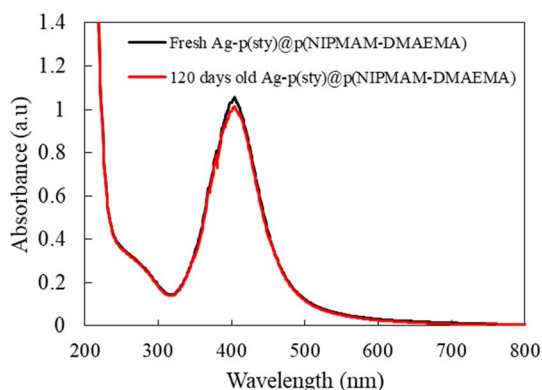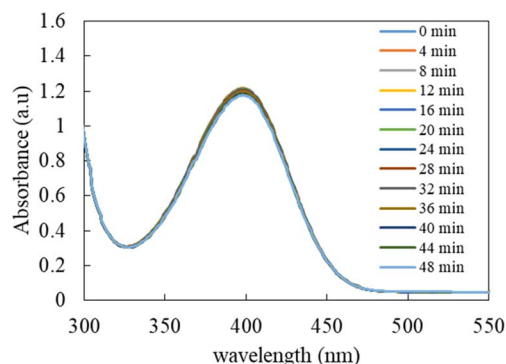
Fig. 7 Time-dependent UV–visible spectrophotometric analysis of the reduction of 0.06 mM 4-NPh by 15 mM NaBH$_4$ in an aqueous medium in the absence of the Ag-p(sty)@p(NIPMAM–DMAEMA) hybrid microgels.

Fig. 9 Time-dependent UV–visible spectrophotometric analysis of the reduction of 0.06 mM 4-NPh to 4-APh by 15 mM NaBH$_4$ in water in the presence of 0.2020 mg mL^{-1} Ag-p(sty)@p(NIPMAM–DMAEMA) pure microgels.

is due to the conversion of 4-NPh into 4-APh. In order to validate the catalytic activity of the Ag nanoparticles, the reduction of 4-NPh was executed by using pure p(sty)@p(NIPMAM–DMAEMA) microgels; as displayed in Fig. 8, no appreciable variation in absorbance was observed. The minor decline in absorbance may be due to the adsorption of 4-NPh to the pure microgel system. These controlled experiments demonstrate that pure p(sty)@p(NIPMAM–DMAEMA) microgel particles are not the catalyst while Ag nanoparticles present in the p(sty)@p(NIPMAM–DMAEMA) microgel are the true catalyst.

The UV-vis spectra for 4-NPh reduction in the presence of Ag-p(sty)@p(NIPMAM–DMAEMA) recorded at various reaction times are shown in Fig. 9. To prevent any interference of the plasmonic feature of silver nanoparticles in absorption spectra, the quantity of Ag-p(sty)@p(NIPMAM–DMAEMA) in the reaction mixture was maintained very low in comparison with the *p*-nitrophenol concentration. As depicted in Fig. 9, the absorbance of 4-NPh gradually decreased over time, which confirms the swift reduction of 4-NPh to 4-APh.

3.5 Kinetic aspects of 4-NPh reduction

The evolution of the reaction was examined by assessing the decrease in the absorbance of *p*-nitrophenolate ions at 398 nm
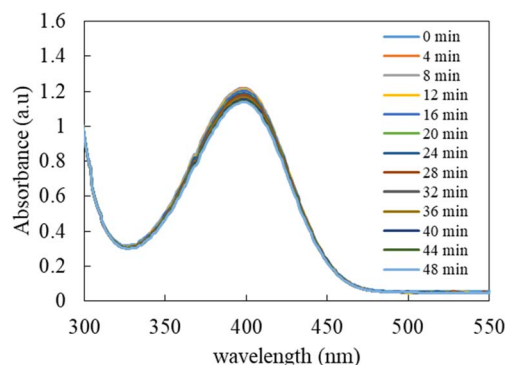
over a constant time interval of 1.5 min, and the data obtained was then used to determine the kinetic parameters. The content of NaBH$_4$ in the reaction mixture was kept 250 times greater than that of 4-NPh during the kinetic studies. Thus, pseudo-first-order kinetics modeling was applied to calculate the value of k_{app}. The mathematical expression of the model can be written as below:

$$\ln\left(\frac{C_t}{C_0}\right) = -k_{app}t \qquad (1)$$

where C_0 is the molarity of 4-NPh ions present at zero time, and C_t is the molarity at any given time t. The fraction A_t/A_0 was used to calculate the ratio C_t/C_0 for the reduction of 4-NPh. The k_{app} value was evaluated from the slope of the straight line represented by eqn (1). A plot depicting the $\ln(C_t/C_0)$ *versus* time curves of the catalytic reduction of 4-NPh to 4-APh in water using 0.06 mM 4-NPh and 15 mM NaBH$_4$ at 14 °C in the presence of different doses of Ag-p(sty)@p(NIPMAM–DMAEMA) system is displayed in Fig. 10. Clearly, each curve has three different segments. In the first segment of each curve, there is no change in the value of $\ln(C_t/C_0)$ over time which shows that

Fig. 8 Time-dependent UV–visible spectrophotometric analysis of the reduction of 0.06 mM 4-NPh by 15 mM NaBH$_4$ in water in the presence of p(sty)@p(NIPMAM–DMAEMA) pure microgels.
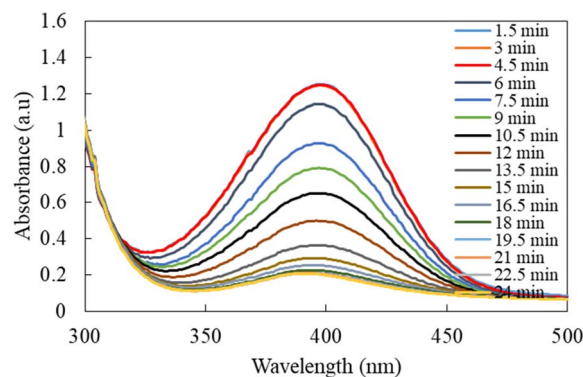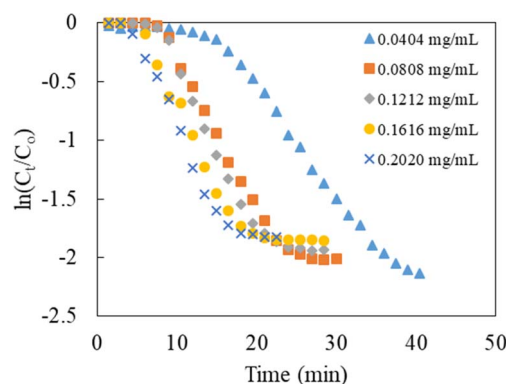

Fig. 10 Plot of $\ln(C_t/C_0)$ *versus* time for the catalytic reduction of 4-NPh (0.06 mM) to 4-APh in water medium using NaBH$_4$ (15 mM) in the presence of 0.0404–0.202 mg mL^{-1} Ag-p(sty)@p(NIPMAM–DMAEMA) hybrid microgel at 14 °C.

Table 1 Apparent rate constants (k_{app}) and half-life times ($t_{1/2}$) for the catalytic reduction of 0.06 mM 4-NPh in the presence of different concentrations of Ag-p(sty)@p(MIPMAM-DMAEMA) with 15 mM NaBH$_4$ at 14 °C

Catalyst dose (mg mL^{-1})	k_{app} (min^{-1})	$t_{1/2}$ (min)
0.0404	0.0915	7.57
0.0808	0.1170	5.92
0.1212	0.1316	5.27
0.1616	0.1364	5.08
0.2020	0.1507	4.60

reduction did not occur. This is referred to as the induction time/delay period.[45] A number of researchers have previously documented the observation of induction time for the reduction of 4-NPh using metal nanoparticles stabilized in polymeric microgel systems.[46,47] The induction time may be caused due to following phenomena: (i) the slow diffusion of 4-NPh from the outside bulk medium to the polymer cage on the inside; (ii) the creation of a silver oxide coating over the silver nanoparticles; or (iii) the reaction between NaBH$_4$ and O$_2$ in water during catalysis. During this period, the catalyst gets activated, and no reduction takes place. Thus, the $\ln(C_t/C_0)$ value remains constant during the initial stage of catalysis. After the initial phase, the $\ln(C_t/C_0)$ value shows a linear decline over time in the subsequent segment. This decline is attributed to the depletion of p-nitrophenol (4-NPh). In the last segment, $\ln(C_t/C_0)$ becomes independent of time again, indicating the completion of the reaction. The k_{app} values were calculated from the gradient of the second segment of the $\ln(C_t/C_0)$ versus t plots at different doses of Ag-p(sty)@p(NIPMAM-DMAEMA) and are listed in Table 1. The value of apparent half-life time ($t_{1/2}$) for the reduction of p-nitrophenol was determined from k_{app} by using the first-order half-life equation ($t_{1/2} = 0.693/k_{app}$). The catalytic conversion of 4-NPh to 4-APh was performed by using 0.06 mM 4-NPh and 15 mM NaBH$_4$ in an aqueous medium in the presence of different contents of Ag-p(sty)@p(NIPMAM-DMAEMA) hybrid microgels in order to study the effect of catalyst dosage on the values of k_{app} and $t_{1/2}$ of the catalytic reduction of 4-NPh. The values of k_{app} and $t_{1/2}$ for the reduction of 0.06 mM 4-NPh by 15 mM NaBH$_4$ using various concentrations of Ag-p(sty)@p(NIPMAM-DMAEMA) are given in Table 1. The value of k_{app} rose with increasing content of Ag-p(sty)@p(NIPMAM-DMAEMA), as shown in Fig. 11 and 12. Table 1 also indicates a decrease in the half-life period with an increase in Ag-p(sty)@p(NIPMAM-DMAEMA) concentration, which can be explained by the increase in k_{app}.

The reduction of 4-NPh by NaBH$_4$ in water medium has become a standard reaction to check the catalytic ability of Ag nanoparticles present in a polymeric system, and the variation of concentration of NaBH$_4$ and substrate is widely reported by our group.[48]

To check whether the prepared hybrid microgel particles are effective catalysts for the reduction of other nitroaromatic systems, the reduction of different nitroarenes was tested by using NaBH$_4$ as the hydrogen source in the aqueous medium. The catalytic reduction of nitroarenes by Ag nanoparticles
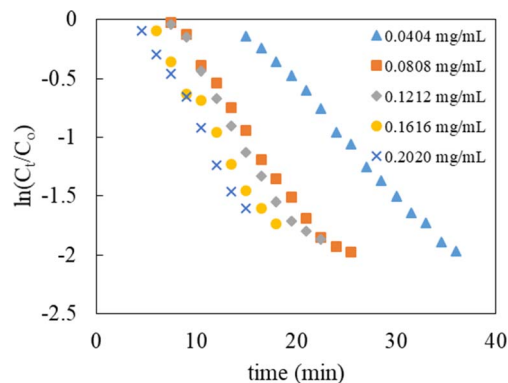

Fig. 11 Graph of $\ln(C_t/C_0)$ versus post-induction time for the catalytic reduction of 4-NPh (0.06 mM) to 4-APh in water medium using NaBH$_4$ (15 mM) in the presence of 0.0404–0.202 mg mL^{-1} Ag-p(sty)@p(NIPMAM-DMAEMA) hybrid microgel at 14 °C.
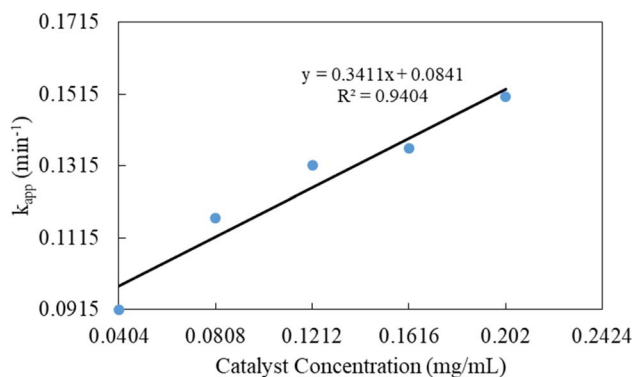

Fig. 12 Plot of k_{app} vs. concentration of Ag-p(sty)@p(NIPMAM-DMAEMA) for the catalytic reduction of 4-NPh (0.06 mM) to 4-APh in an aqueous medium using NaBH$_4$ (15 mM) in the presence of 0.0404–0.202 mg mL^{-1} Ag-p(sty)@p(NIPMAM-DMAEMA) hybrid microgel at 14 °C.

loaded into the polymeric microgels followed the Langmuir–Hinshelwood mechanism; that is, reactant molecules diffuse via open polymeric networks towards the silver nanoparticles present in the sieves of the polymeric system and react with each other on the metal surface to give products that finally diffuse out of the polymeric network, as described in the literature.[49] During the experiments, the concentrations of all the nitroarenes, sodium borohydride, and catalysts were kept the same, as shown in Fig. S2 (ESI).† The fall in absorbance at the λ_{max} of each substrate with time indicates the transformation of nitroarenes into corresponding aryl amines in the presence of the Ag-p(sty)@p(NIPMAM-DMAEMA) catalyst. The summary of the catalytic reduction of different nitroarenes in a water medium by the Ag-p(sty)@p(NIPMAM-DMAEMA) hybrid microgel is also given in Table S1.†

4. Conclusions

In this study, p(sty)@(NIPMAM-DMAEMA) particles with a highly narrow size distribution were successfully obtained in

two steps by seed-mediated free-radical precipitation polymerization in water. The p(sty) core particles were found to be insensitive to temperature, while p(sty)@(NIPMAM-DMAEMA) was thermoresponsive with a VPTT around the physiological temperature in water. Spherical silver nanoparticles with diameters between 10 and 15 nm were successfully formed in the shell region of the p(sty)@p(NIPMAM-DMAEMA) core/shell microgels. The fabricated silver nanoparticles were very stable for a long period of time because of the donor–acceptor interaction of the tertiary amino and carbonyl groups of the DMAEMA moieties in p(sty)@p(NIPMAM-DMAEMA) with the fabricated silver nanoparticles. The resultant hybrid microgels demonstrated excellent catalytic properties by efficiently transforming toxic 4-NPh into less-toxic and highly useful 4-APh. The k_{app} value increased with an increase in catalyst concentration, which indicates the occurrence of the reaction on the surface of the nanosilver. This hybrid system is inexpensive and can be used for the catalysis of various other organic transformations. This work may guide researchers to produce nanoparticles of other metals, like Au, Pt, Pd and Ru, inside the shell region of p(sty)@p(NIPMAM-DMAEMA) core/shell microgels, and the synthesized hybrid microgels may be used for catalysis in environmental and industrial applications.

Data availability

The data that support the findings of this study are available with the first author upon reasonable request.

Conflicts of interest

Authors declare no conflict of interest.

Acknowledgements

References

1 C. You, C. Han, X. Wang, Y. Zheng, Q. Li, X. Hu and H. Sun, *Mol. Biol. Rep.*, 2012, **39**, 9193–9201.

2 B. Choi, H. H. Lee, S. Jin, S. Chun and S. H. Kim, *Nanotechnology*, 2007, **18**, 075706.

3 D. Chen, X. Qiao, X. Qiu and J. Chen, *J. Mater. Sci.*, 2009, **44**, 1076–1081.

4 S. Iyahraja and J. S. Rajadurai, *AIP Adv.*, 2015, **5**, 057103.

5 E. Abbasi, M. Milani, S. F. Alvi, M. Kouhi, A. Akbarzadeh, H. T. Nasrdbi, P. Nikasa, S. W. Joo, Y. Hanifehpour, K. N. koshki and M. Samiei, *Crit. Rev. Microbiol.*, 2016, **42**, 173–180.

6 Z. H. Farooqi, K. Naseem, R. Begum and A. Ijaz, *J. Inorg. Organomet. Polym. Mater.*, 2015, **25**, 1554–1568.

7 K. Naseem, R. Begum, W. Wu, A. Irfan, A. G. Al-Sehami and Z. H. Farooqi, *J. Cleaner Prod.*, 2019, **211**, 855–864.

8 K. Midha, G. Singh, M. Nagpal and S. Arora, *Nanosci. Nanotechnol.–Asia*, 2016, **6**, 82–91.

9 S. Gajbhiye and S. Sakharwade, *J. Cosmet., Dermatol. Sci. Appl.*, 2016, **6**, 48–53.

10 M. Korani, E. Ghazizadeh, S. Korani, Z. Hami and A. M. Bardbori, *Eur. J. Nanomed.*, 2015, **7**, 51–62.

11 G. G. Carbone, A. Serra, A. Buccolieri and D. Manno, *Heliyon*, 2019, **5**, e02887.

12 K. V. Alex, P. T. Pavai, R. Rugmini, M. S. Prasad, K. Kamakshi and K. C. Sekhar, *ACS Omega*, 2020, **5**, 13123–13129.

13 H. I. O. Gomes, C. S. M. Martins and J. A. V. Prior, *Nanomaterials*, 2021, **11**, 964.

14 S. Zahid, A. K. Alzahrani, N. Kizibash, J. Ambreen, M. Ajmal, Z. H. Farooqi and M. Siddiq, *RSC Adv.*, 2022, **12**, 33215–33228.

15 N. Duran, P. D. Marcato, D. I. H. Souza, O. L. Alwes and E. Esposito, *J. Biomed. Nanotechnol.*, 2007, **3**, 203–208.

16 T. Bruna, F. M. Bravo, P. Jara and N. Caro, *Int. J. Mol. Sci.*, 2021, **22**, 7202.

17 A. M. Elgorban, A. E. M. El-Samawaty, M. A. Yassin, S. R. Sayed, S. F. Adil, K. M. Elhindi, M. Bakri and M. khan, *Biotechnol. Biotechnol. Equip.*, 2016, **30**, 56–62.

18 Z. A. Ratan, M. F. Haidere, M. D. Nurunnabi, S. M. Shahriar, A. J. S. Ahammad, Y. Y. Shim, M. J. T. Reaney and J. Y. Cho, *Cancers*, 2020, **12**, 855.

19 S. Galdiero, A. Falanga, M. Vitiello, M. Cantisani, V. Marra and M. Galdiero, *Molecules*, 2011, **16**, 8894–8918.

20 Z. H. Farooqi, S. R. Khan, T. Hussain, R. Begum, K. Ejaz, S. Majeed, M. Ajmal, F. Kanwal and M. Siddiq, *Korean J. Chem. Eng.*, 2014, **31**, 1674–1680.

21 R. Begum, Z. H. Farooqi, A. H. Aboo, E. Ahmed, A. Sharif and J. Xiao, *J. Hazard. Mater.*, 2019, **377**, 399–408.

22 Z. Zhang, L. Zhang, S. Wang, W. Chen and Y. Lei, *Polymer*, 2001, **42**, 8315–8318.

23 Y. Lu, Y. Mei, M. Schrinner, M. Ballauff, M. W. Moller and J. Breu, *J. Phys. Chem. C*, 2007, **111**, 7676–7681.

24 L. Jin, S. P. Yang, H. X. Wy, W. W. Huang and Q. Tian, *J. Appl. Polym. Sci.*, 2008, **108**, 4023–4028.

25 J. Zheng and R. M. Dickson, *J. Am. Chem. Soc.*, 2002, **124**, 13982–13983.

26 S. K. Ghosh, S. Kundu, M. Mandal, S. Nath and T. Pal, *J. Nanopart. Res.*, 2003, **5**, 577–587.

27 J. Xu, X. Han, H. Liu and Y. Hu, *Colloids Surf., A*, 2006, **273**, 179–183.

28 D. Radziuk, A. Skirtach, G. Sukhorukov, D. Shchukin and H. Mohwald, *Macromol. Rapid Commun.*, 2007, **28**, 848–855.

29 K. Naseem, R. begum, Z. H. Farooqi, W. Wu and A. Irfan, *Appl. Organomet. Chem.*, 2020, **34**, e5742.

30 Z. H. Farooqi and M. Siddiq, *J. Dispersion Sci. Technol.*, 2015, **36**, 423–429.

31 R. Begum, J. Najeeb, G. Ahmad, W. Wu, A. Irfan, A. G. Al-sehemi and Z. H. Farooqi, *React. Funct. Polym.*, 2018, **132**, 89–97.

32 S. Iqbal, C. Zahoor, S. Musaddiq, M. Hussain, R. Begum, A. Irfan, M. Azam and Z. H. Farooqi, *Ecotoxicol. Environ. Saf.*, 2020, **202**, 110924.

33 S. Rehman, A. R. Khan, A. Shah, A. Badshah and M. Siddiq, *Colloids Surf., A*, 2017, **520**, 826–833.

34 X. Huang, Y. Xiao, W. Zhang and M. Lang, *Appl. Surf. Sci.*, 2012, **258**, 2655–2660.

35 N. S. Reddy, S. Eswaramma, I. Chung, K. S. V. K. Rao, P. Ramesh and A. C. Dekhar, *Int. J. Polym. Mater. Polym. Biomater.*, 2019, **68**, 870–880.

36 L. Zha, J. Hu, C. Wang, S. Fu, A. Elaissari and Y. Zhang, *Colloid Polym. Sci.*, 2002, **280**, 1–6.

37 K. Naseem, Z. H. Farooqi, R. Begum, W. Wu, A. Irfan and A. G. Al-sehemi, *Macromol. Chem. Phys.*, 2018, **219**, 1800211.

38 K. Naseem, R. Begum, W. Wu, M. Usman, A. Irfan, A. G. Al-sehemi and Z. H. Farooqi, *J. Mol. Liq.*, 2019, **277**, 522–531.

39 J. Zhou and X. Zha, *React. Funct. Polym.*, 2019, **137**, 46–56.

40 M. Arif, A. Rauf and T. Akhter, *RSC Adv.*, 2024, **14**, 19381–19399.

41 X. Hu, Z. Tong and L. A. Lyon, *Colloid Polym. Sci.*, 2011, **289**, 333–339.

42 Z. H. Farooqi, N. Tariq, R. Begum, S. R. Khan, Z. Iqbal and A. Khan, *Turk. J. Chem.*, 2015, **39**, 576–588.

43 S. Iqbal, S. Musaddiq, R. Begum, A. Irfan, Z. Ahmad, M. Azam, J. Nisar and Z. H. Farooqi, *Z. Phys. Chem.*, 2021, **235**, 1701–1719.

44 K. Naseem, Z. H. Farooqi, M. Z. U. Rehman, M. A. U. Rehman and M. Ghufran, *Rev. Chem. Eng.*, 2019, **35**, 285–309.

45 Z. H. Farooqi, S. Iqbal, S. R. Khan, F. Kanwal and R. Begum, *E-Polymers*, 2014, **14**, 313–321.

46 M. Ajmal, Z. H. Farooqi and M. Siddiq, *Korean J. Chem. Eng.*, 2013, **30**, 2030–2036.

47 A. Pich, A. Karak, Y. Lu, A. K. Ghosh and H. J. P. Adler, *J. Nanosci. Nanotechnol.*, 2006, **6**, 3763–3769.

48 R. Begum, Z. H. Farooqi, E. Ahmad, K. Naseem, S. Ashraf, A. Sharif and R. Rehan, *Appl. Organomet. Chem.*, 2017, **31**, e3563.

49 R. Begim, Z. H. Zahoor, Z. Butt, Q. Wu, W. Wu and A. Irfan, *J. Environ. Sci.*, 2018, **72**, 43–52.